Electrical characterization with atomic force microscopy and low temperature transport properties of boric acid doped polyaniline with Fe_3O_4 nanoparticles composites

A. BALLESTAR[a], F. YAKUPHANOGLU[b,c*], B. FILIZ ŞENKAL[d], M. MUÑOZ[e], W. A. FAROOQ[c]
[a]*Laboratorio de Física de Sistemas Pequeños y Nanotecnología, Consejo Superior de Investigaciones Científicas (CSIC), Serrano 144, Madrid 28006 Spain*
[b]*Physics Department, Faculty of Science, Firat University, Elazig, Turkey*
[c]*Department of Physics and Astronomy, College of Science,King Saud University, Riyadh, Kingdom of Saudi Arabia*
[d]*Department of Chemistry, Faculty of Arts and Sciences, İstanbul Technical University, 34469, Maslak, Istanbul, Turkey*
[e]*Instituto de Física Aplicada, Consejo Superior de Investigaciones Científicas (CSIC), Serrano 144, Madrid 28006 Spain*

The electrical charge transport properties of the boric acid doped polyaniline with Fe_3O_4 nanoparticles composites have been investigated in the temperature range of 35 K to 300 K. The microstructure and electrical conductivity properties of the polymer nanocomposites were further analyzed by scanning electron microcopy (SEM) and atomic force microscopy (AFM). The electrical conductivity of the composites changes with Fe_3O_4 dopant. This suggests that interactions between the polymer matrix and Fe_3O_4 nanoparticles take place. The characteristic Mott temperature confirms the highest conductivity for the composite with 5%wt dopant. The charge transport mechanism of the composites varies from three dimensional hopping to tunneling mechanism. It is demonstrated that the boric acid doped polyaniline with Fe_3O_4 nanoparticles composites are typical organic semiconductors.

(Received January 24, 2011; accepted February 17, 2011)

Keywords: Fe_3O_4, Electrical properties, Organic semiconductor, Nanocomposites

1. Introduction

Polymeric nanocomposites have potential applications in electrochromic devices [1], nonlinear optical systems [2], light emitting diodes [3], photodiodes and photovoltaic solar cells [4], gas and vapor sensors [5], and magnetic storage materials [6]. Polyaniline was one of the most important conducting polymers due to its ease of synthesis, environmental stability and simple doping/dedoping chemistry [7,8]. Among the inorganic magnetic nanoparticles, Fe_3O_4 nanoparticles had received great attention because of their interesting magnetic properties as well as extensive potential applications in color imaging, magnetic recording media, soft magnetic materials and ferrofluids [9–11]. A large number of articles have been published reporting on the polymeric nanocomposites, i.e., PANI or polypyrrole composites containing nanoparticles such as TiO_2 [12,13] and Fe_3O_4 [14–18], because, nanocomposites exhibit improved chemical and physical properties for technological applications.

The aim of the present work is to synthesize polymer nanocomposites in which Fe_3O_4 are well dispersed at various concentrations to obtain new organic semiconductors.

2. Experimental details

2.1 Preparation of Fe_3O_4 particles

For this study, aniline, boric acid, ammonium persulphate (APS), $FeCl_3 \cdot 6H_2O$ and $FeCl_2 \cdot 4H_2O$ were obtained from Aldrich. Aniline was distilled under reduced pressure.

Fe_3O_4 particles were prepared by precipitation oxidation method according to the literature [19]. The detailed process could be described as follows. A mixture of 10.534 g of $FeCl_3 \cdot 6H_2O$ and 4.276 g of $FeCl_2 \cdot 4H_2O$ dissolved in 80 ml of deionized water was placed in a 250 ml three-necked round bottom flask, following by the quick droplet-addition of 40 ml of an aqueous solution containing 25 ml ammonia. The reaction mixtures were stirred for 12 h at room temperature. The resulting black precipitate suspension was filtered and washed with water. Then it was dried under vacuum for 24 h at room temperature.

Preparation and measurements of polyaniline-magnetite composites

In this study, different weight percentage of magnetite was used 5%, 8%, 10% and 50%wt, respectively. The magnetite particles were dispersed in 10 mL of distilled water by bath sonication for 2 h. Aniline (1 g) and 1 g of boric acid in 50 mL of water was added into the magnetite

containing mixture. The reaction content was dispersed by bath sonication for 1 h. Then, 3 g of ammonium persulfate in 40 mL of water was added dropwise (15–20 min interval) at 0 ^{0}C. The reaction mixture was kept for 24 hr at room temperature. The reaction mixture was filtered, washed with excess of water, and finally with ethanol. The samples were dried at room temperature under vacuum. The products were characterized by FT-IR. The main characteristic bands of doped polyaniline are assigned as follows: the bands at 1575 and 1492 cm^{-1} are attributable to C=N and C=C stretching mode for the quinoid and benzenoid rings. The bands at 1277 and 1240 cm^{-1} have been attributed to C-N stretching mode of benzenoid ring and band at 1112 cm^{-1} is due to a plane bending vibration of C-H. Through studying IR spectra of PANI/Fe_3O_4 composites, Kryszewski and Jeszka [20] have pointed out that the bands at 783 and 878 cm^{-1} are due to OH groups bound to the surface of Fe_3O_4 particles.

The synthesized polymer nanocomposites were prepared in the form of disc under 10 ton. Electrical conductivity was measured as a function of temperature by an alternating polarity method to eliminate electrical polarization, triboelectric and piezoelectric effects using KEITHLEY 6517A electrometer.

3. Results and discussion

3.1. Morphology of boric acid polyaniline/magnetite composites

Fig. 1 shows the scanning electron microcopy photograph. As seen in Fig. 1, the Fe_3O_4 nanoparticles are rarely dispersed in the polymer matrix. Also, we have investigated simultaneously the surface topography of the polymer and the local resistance distribution at room temperature by atomic force microscope (AFM). We have used an AFM Solver P47 from, NTMDT working in spreading resistance mode. In this mode a conductive AFM tip is in direct contact with the sample surface. A voltage bias is applied to the tip and the resulting current through the sample-tip junction is measured as a function of the tip position on the surface simultaneously with the topography of the sample. Silicon AFM probes (MikroMasch NSC14/Ti-Pt) were used for all reported data. The tips with nominal force constant of approximately 5 N/m have a Ti-Pt coating in order to perform the conductive measurements. The thickness of Pt coating is about 10 nm and the Ti under layer has a thickness of 20 nm and increase adhesion to the silicon cantilever. The resulting tip has a curvature radius of 40 nm consequently the contact area between the tip and polymer is about 150 nm^2. Fig. 2 shows the topography and current distribution in the surface of the polymer nanocomposite for 10%wt dopant. Fig. 2(a) is the topography recorded in contact mode. Fig. 2 (b) shows the current distribution when we apply a voltage bias of 5 Volts between the AFM tip and the polymer surface. Bright areas of the picture correspond to higher current in the tip-polymer junction what means that the conductivity of the polymer is higher at this point. We have also investigated the current-voltage characteristics at different points on the polymer nano composite. In this case, we fix the position of the AFM tip in the point of interest while we sweep the voltage bias and record the current flowing. Fig. 3 shows the current-voltage characteristics of the polymer in one of the bright areas of Fig. 2 b. These current voltage characteristics are typical for semiconducting polymers.

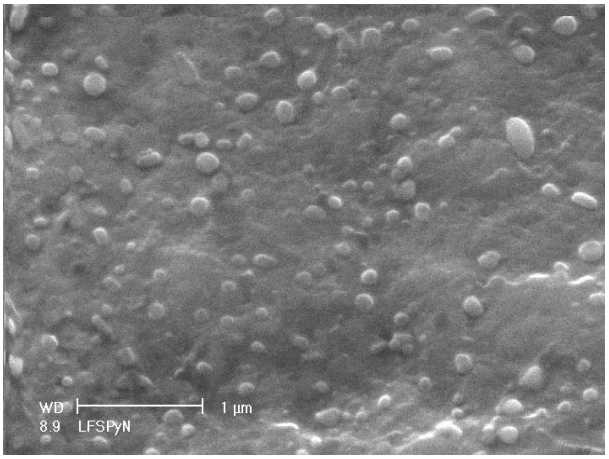

Fig. 1. Microstructure graph of the nanocomposite.

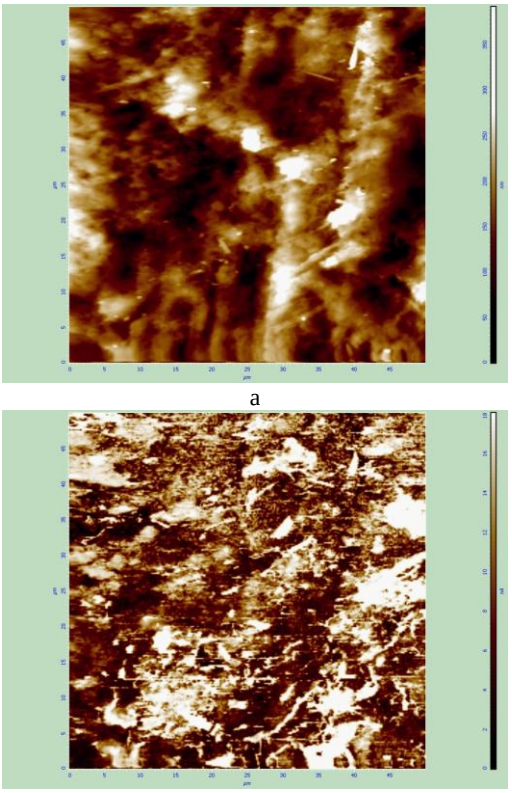

a

b

Fig. 2. a) Topography of the polymer sample recorded by AFM in contact mode; b) current distribution (V_{bias}= 5 Volts) recorded at the same time that the topography data.

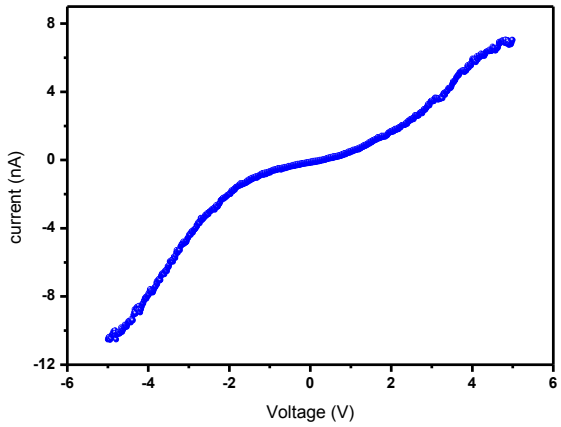

Fig. 3. Current voltage characteristics of the polymer measured on one of the bright areas (high current) of the current distribution shown in Fig. 2 b.

3.2. Electrical conductivity properties of boric acid polyaniline/magnetite composites

Fig. 4 shows the plots of the electrical conductivity dependence of temperature of the composites at lower temperatures. The electrical conductivity of the composites decreases with decreasing temperature, which is the typical behavior of semiconductor materials. The electrical conductivity of the composites increases for 5% and 8%wt Fe_3O_4 dopants and then, decreases as we increase more the dopant concentration. For 5% magnetit dopant, the composite has the highest electrical conductivity. After 10%wt Fe_3O_4 dopant, the electrical conductivity of the composite is lower than that of boric acid doped polyaniline. The electrical conductivity of the 5% and 8% composites are higher than that of the polymer. The electrical conductivity of the composites follow of the order of $\sigma_{5\%MAGN} > \sigma_{8\%MAGNA} > \sigma_{0\%MAGN} > \sigma_{10\%MAGN.} > \sigma_{50\%MAGN}$ The electrical conductivity decreases for 10 and 50%wt dopants. The decrease in conductivity is due to the interactions between the polymer matrix and Fe_3O_4 nanoparticles because these interactions increases the charge carrier scattering and therefore the conductivity of the nanocomposites decrease with increasing the Fe_3O_4 content.

As seen in Fig. 4, the conductivity plots indicate two linear regions having different slopes, suggesting that two charge transport mechanisms are possible for the polymer composites. For the first region, the variable hopping conductivity mechanism is defined as follows [21],

$$\sigma = \sigma_o \, exp\left[-\left(\frac{T_o}{T} \right)^{1/n} \right] \tag{1}$$

where n is a constant which is related to the dimensionality of the process, 2 (one-dimensional variable range hopping), 3 (two-dimensional variable hopping), 4 (three-dimensional variable hopping). σ_o is the conductivity at finite temperature and T_o is the characteristic temperature that determines the thermally activated hopping among localized states at different energies [21]. It is evaluated that the first region indicates the existence of the three-dimensional hopping conductivity, but in second region conductivity is controlled by tunneling mechanism. The plots of $\ln\sigma T^{1/2}$ vs $T^{-1/4}$ of the composites are shown in Fig. 5. The plots indicate linearity in the investigated temperature range. This suggests that the variable hopping mechanism (3D-VRH) is dominant in the first region and thus, Eq. 1 can be rewritten for three dimensional hopping conductivity as follows,

$$\sigma = \sigma_o / \sqrt{T} \, exp\left[-\left(\frac{T_o}{T} \right)^{\frac{1}{4}} \right] \tag{2}$$

where σ_o and T_o are given by the following equations [21],

$$\sigma_o = e^2 \left[\frac{9 L_{Loc} N(E_F)}{8\pi kT} \right]^{1/2} \nu_{ph} \tag{3}$$

$$T_o = \frac{18}{kN(E_F) L_{Loc}^3} \tag{4}$$

where L_{Loc} is localization length and $N(E_F)$ is the density of states at Fermi level. The values of L_{Loc} and $N(E_F)$ are found from solution of equations 3 and 4 as follows,

$$L_{Loc} = \frac{4.44x10^{-2}}{\sigma_o \sqrt{T_o}} cm \tag{5}$$

and

$$N(E_F) = 2.12x10^9 \sigma_o^3 \sqrt{T_o} cm^{-3} eV^{-1} \tag{6}$$

The average hopping distance R_{hop} between two sites and the hopping activation energy, W_{hop} *is* given by,

$$R_{hop} = \left[\frac{9 L_{Loc}}{8\pi kTN(E_F)} \right]^{1/4} \tag{7}$$

and

$$W_{hop} = \frac{3}{4\pi R_{hop}^3 N(E_F)} \tag{8}$$

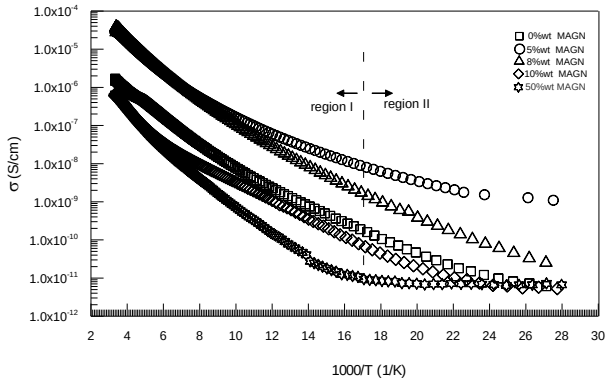

Fig. 4. The variation of dc conductivity with temperature of the composites.

The electrical parameters of the three-dimensional hopping conductivity for the composites were determined via Fig. 5 and are given in Table 1. The obtained parameters confirm the presence of 3D-VRH mechanism in the composites. As seen in Table 1, the characteristic Mott temperature changes with Fe_3O_4 dopants. The nanocomposite for 5%wt dopant has the smallest value of T_o. This suggests that this composite has the highest conductivity.

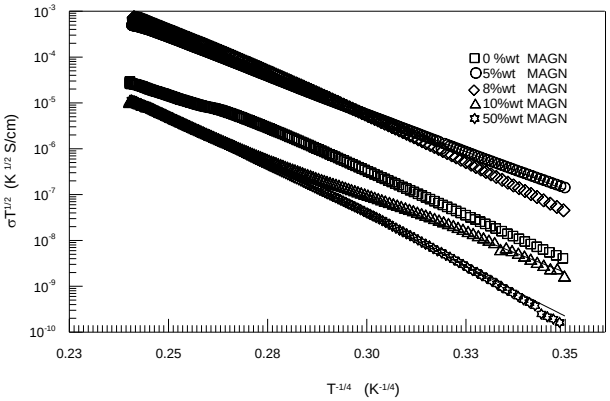

Fig. 5. Plot of 3D-VRH conductivity of the composite.

Table 1. The electrical parameters of the composites.

Composite	*0% MAGN*	*5% MAGN*	*8% MAGN*	*10% MAGN*	*50% MAGN*
T_0 (K)	$6.42x10^3$	$5.82x10^3$	$7.72x10^3$	$6.05x10^3$	$1.01x10^4$
σ_{01} (S/cm)	8.44×10^3	5.13×10^4	1.38×10^6	1.34×0^3	4.34×10^5
L_{Loc} (cm)	6.55×10^{-8}	1.13×10^{-8}	3.65×10^{-10}	4.25×10^{-7}	1.01×10^{-9}
$N(E_F)$ (eV^{-1} cm^{-3})	1.02×10^{23}	2.185×10^{25}	4.93×10^{29}	3.97×10^{20}	1.74×10^{23}
W (meV) at 100 K	6.28	6.13	6.57	6.19	125.8
R(cm) at 100 K	7.18×10^{-8}	1.21×10^{-8}	4.18×10^{-10}	4.59×10^{-7}	2.21×10^{-8}

As point out by Mott [21], the probability that a carrier hops to spatially more distant but energetically closer sites increase as temperature is lowered, because the VRH is a phonon-assisted process. When the phonon energy is not enough to support hop to the nearest available site, the carrier will look further a field for an energetically closer site [21]. This event also decreases the activation energy for the hopping process. This mechanism is obtained by optimizing the hopping probability and assuming a slowly variation of the density of states (DOS) in the vicinity of the Fermi level. We have successfully tested a universal behavior of the conductivity in VRH regime and it is assumed the charge carriers move away along a path determined by the optimal rate of pair hopping from one localized state to another. Band conduction does not take place in this model as extended states are far away from the Fermi level. In the variable range hopping (VRH) process [22-24], it becomes favorable for an electron to jump from one localized state to another where there is an overlap of the wave functions. The difference in the eigen energies is compensated by the absorption or emission of phonons. When the temperature is low enough so that carriers cannot be excited into one of the allowed bands, in which carriers hop from occupied to unoccupied sites which are located within the band gap. Such a hopping mechanism may occur when the density of localized states is high enough to allow a non-negligible overlap of the individual wave functions. It is assumed all electronic states to be localized with phonon assisted transitions between them. Such a mechanism is consistent with the existence of a high density of states in the semiconductor energy gap [25]. At lower temperatures, <60 K, the tunneling contribution to the conductivity is dominant in the composites. This mechanism has been reported earlier for the other conjugated polymers [26-28].

4. Conclusions

The electrical charge transport properties of the boric acid doped polyaniline with Fe_3O_4 nanoparticles composites have been investigated in the temperature range of 35 K to 300 K. The electrical conductivity of the composites changes with Fe_3O_4 dopant. The electrical conductivity of the composites is controlled by three-dimensional hopping and tunneling mechanism. The polymer nanocomposites exhibit semiconductor behavior.

Acknowledgments

This work was supported by the National Boron Research Institute (BOREN) (Project Number: BOREN-2006-26-Ç25-19) and King Saud University under grant:

KSU-VPP-102. Authors wishes to thank BOREN and KSU.

References

[1] P. K. Shen, H. T. Huang, A. C. C. Tseung, J. Electrochem. Soc. **139**, 1840 (1992).
[2] X. Peng, Y. Zhang, J. Yang, B. Zou, P. Xia, J. Phys. Chem. **96**, 3412 (1992).
[3] V. L. Colvin, M. C. Schlamp, A. P. Alivisatos, Nature **370**, 354 (1994).
[4] A. W. Olsen, Z. H. Kafafi, J. Am. Chem. Soc. **113**, 7758 (1993).
[5] D. Godovsky, A. Volkov, V. Sukharev, M. Moskvina, Analyst **118**, 997 (1994).
[6] I. Anton, J. Magn. Magn. Mater. **85**, 219 (1990).
[7] N.-R. Chiou, A. J. Epstein, Adv. Mater. **17**, 1679 (2005).
[8] F. Yakuphanoglu, R. Mehrotra, A. Gupta, Manuel Munoz, Journal of Applied Polymer Science, Article in Press (2009).
[9] L. Xu, W. Zhang, Y. Ding, Y. Peng, S. Zhang, W. Yu, Y. Qian, J. Phys. Chem. B **108**, 10859 (2004).
[10] J. M. De Teresa, A. Fern´andez-Pacheco, L. Morellon, J. Orna, J. A. Pardo, D. Serrate, P. A. Algarabel, M.R. Ibarra, Microelectron. Eng. **84**, 1660 (2007).
[11] C.-L. Chiang, C.-S. Sung, T.-F.Wu, C.-Y. Chen, C.-Y. Hsu, J. Chromatogr. B **822**, 54 (2005).
[12] J. S. Salafsky, Phys. Rev. B. **59**, 10885 (1999); S. J. Su, N. Kuramoto, Synth. Met. **114**, 147 (2000); L. J. Zhang, M. X. Wan, J. Phys. Chem. B **107**, 6748 (2003).
[13] A. Dey, S. De, A. De, S. K. De, Nanotechnology **15**, 1277 (2004).
[14] J. Deng, C. He, Y. Peng, J. Wang, X. Long, P. Li, A. S. C. Chan, Synth. Met. **139**, 295 (2003).
[15] D. G. Shchukim, I. L. Radtchenko, G. B. Sukhorukov, Mater. Lett. **57**, (17432002).
[16] M. Wan, W. Li, J. Polym. Sci. Part A **35**, 2129 (1997); M. Wan, J. Fan, J. Polym. Sci. Part A **36**, 2749 (1998); J. Lin, M. Wan, J. Polym. Sci. Part A **38**, 2734 (2000).
[17] A. Chen, H. Wang, B. Zhao, X. Li, Synth. Met. **139**, 411 (2003); A. Chen, H. Wang, X. Li, Synth. Met. **145**, 153 (2004).
[18] J. Deng, C. He, Y. Peng, J. Wang, X. Long, P. Li, A.S.C. Chan, Synth. Met. **139**, 295 (2003); J. C. Aphesteguy, S. E. Jacobo, Physica B **354**, 224 (2004).
[19] Qi Xiao, Xiaoke Tan, Lingling Ji, Jing Xue, Synthetic Metals **157**, 784 (2007).
[20] M. Kryszewski, J. K. Jeszka, Synth. Met. **94**, 99 (1998).
[21] N. F. Mott, E. A. Davis 1979 Electronic Process in Non-Crystalline Materials (Clarendon Press: Oxford).
[22] I. Morales, M. G. Olayo, G. J. Cruz, M. M. Castillo-Ortega. R. Olayo, J. Poly. ScLPart B, Polymer Physics, **38**, 3247 (2000).
[23] N. F. Mott, E. A. Davis, Electronic Processes in Non-crystalline Materials, Clarendon Press Oxford, (1971).
[24] F. Demichelis, C. F. Pirri, E. Tresso, Phil. Mag. B **65**, 681 (1992).
[25] C. N. Berglund, H. J. Guggenheim, Phys. Rev. **185**, 1022 ~1969.
[26] R. Singh, A. Kaur, K. L. Yadav, D. Bhattacharya Current Appl. Phys. **3**, 235 (2003).
[27] C. O. Yoon, M. Reghu, D. Moses, A. J. Heeger, Y. Cao, T.-A. Chen, X. Wu, R. D. Rieke, Synth. Met. **75**, 229–39 (1995).
[28] M. Reghu, S. V. Subramanyam Solid State Commun.**72**, 325 (1989).

*Corresponding author: fyhanoglu@firat.edu.tr, fyakuphanoglu.v@ksu.edu.sa